FINAL PROGRESS REPORT

COMPUTATIONAL MODELING AND ANALYSIS OF SYNTHETIC JETS

INVESTIGATORS: RAJAT MITTAL (GWU); LOU CATTAFESTA (UF)

STUDENTS SUPPORTED: PRAKIT RAMPUNGGOON, B. R. RAVI, RUPESH B. KOTAPATI, YOGEN UTTURKAR

AGREEMENT: NAG-1-01024
MONITOR: SUSAN GORTON

PERIOD OF PERFORMANCE: MARCH 1, 2001 – MARCH 31, 2005

ACCOMPLISHMENTS

1. Computational Modeling of 3D Synthetic Jets

In the last report we focused on the study of 3D synthetic jets of moderate jet aspect-ratio. Jets in quiescent and cross-flow cases were investigated. Since most of the synthetic jets in practical applications are found to be of large aspect ratio, the focus was shifted to studying synthetic jets of large aspect ratio. In the current year, further progress has been made by studying jets of aspect ratio 8 and infinity. Some other aspects of the jet, like the vorticity flux is looked into apart from analyzing the vortex dynamics, velocity profiles and the other dynamical characteristics of the jet which allows us to extract some insight into the effect of these modifications on the jet performance. Also, efforts were made to qualitatively validate the simulated results with the NASA Langley test cases at higher jet Reynolds number for the quiescent jet case.

1.1 Numerical Methodology

The evolution of zero-net-mass-flux (ZNMF) synthetic jets from a cavity in the absence of crossflow is modeled by the unsteady, incompressible Navier-Stokes equations, written in tensor form as

$$\frac{\partial u_i}{\partial x_i} = 0$$

$$\frac{\partial u_i}{\partial t} + \frac{\partial (u_i u_j)}{\partial x_j} = -\frac{\partial p}{\partial x_i} + \frac{1}{\text{Re}} \frac{\partial^2 u_i}{\partial x_j \partial x_j}$$

where the indices, $i = 1$, 2, 3, represent the x_1 (x), x_2 (y), x_3 (z) directions, respectively, p is the pressure and the components of the velocity vector u are denoted by u_1 (u), u_2 (v) and u_3 (w), respectively. The equations are non-dimensionalized with the appropriate length and velocity scales where Re represents the Reynolds number. The Navier-Stokes equations are discretized using a cell-centered, collocated (non-staggered) arrangement of the primitive variables (u, p). In addition to the cell-center velocities (u), the face-center velocities (U), are also computed. Similar to a fully staggered arrangement, only the component normal to the cell-face is calculated and stored. The face-center velocity is used for computing the volume flux from each cell. The advantage of separately computing the face-center velocities has been initially proposed by Zang, Street and Koseff (1994) and discussed in the context of the current method in Ye at al (2004). The equations are integrated in time using a second-order accurate fractional step method.

In the first step, the pressure field is computed by solving a Poisson equation. A second-order Adams-Bashforth scheme is employed for the convective terms while the diffusion terms are discretized using an implicit Crank-Nicolson scheme which eliminates the viscous stability constraint. The pressure Poisson equation is solved with a Krylov-based approach. The solver uses weighted-averaging of second order central difference scheme and second order upwind scheme for the discretization of convective face velocities. The QUICK scheme (Leonard, 1979) obtained by setting the weighting factor $\theta = 1/8$ is used in some of the present computations. Care has been taken to ensure that the discretized equations satisfy local and global mass conservation constraints as well as pressure-velocity compatibility relations. The code has been rigorously validated by comparisons of several test cases against established experimental and computational data. Details have been presented elsewhere (Najjar and Mittal, 2003).

1.2 Simulations of large aspect ratio synthetic jets

Synthetic jet of aspect ratio 8 is simulated for both the quiescent case as well as jet in a crossflow at jet Reynolds number, Re_j = 300 based on the jet exit area and average jet velocity during the expulsion part of the cycle. The computations are made for a Stokes number, S = 6.84. Existing experimental results are used as basis for the Stokes number selection. A grid size of 105 x 236 x 105 and a large domain size of 320d x 100d x 320d is used for the purpose, where d is the jet exit width. The timestep, Δt, is chosen so as to give a total of 14000 time steps per cycle. Also the cavity shape is now chosen to be more rectangular as is the case in most practical applications. The shape of the cavity has little effect on the jet performance and characteristics as shown earlier by the studies of Utturkar et al.

For the quiescent jet case, the iso-surfaces of vorticity $\sqrt{\omega_x^2 + \omega_z^2}$ are shown in Figure 1 below for the first two phases of the expulsion cycle, viz. the maximum expulsion and the minimum volume phases. Though, the vortex structures does provide a overall view of the nature of the flow in the near exit and the downstream regions of the jet exit plane, the embedded vortical structures are concealed. A better view of such structures is shown in the figure 2 corresponding to the same two phases as in figure 1. This
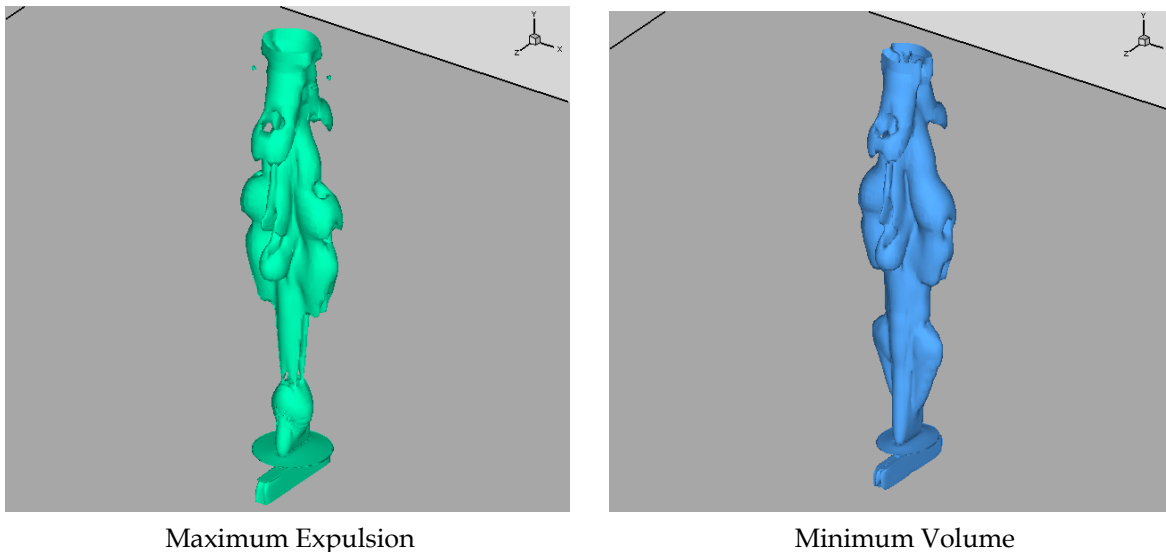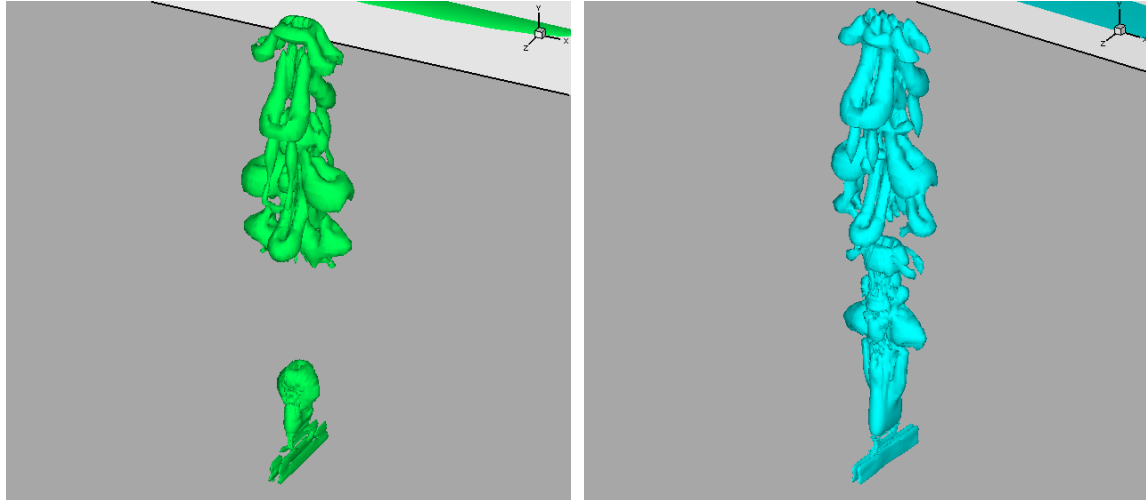

Maximum Expulsion   Minimum Volume

Figure1. Isosurfaces of vorticity for jet aspect ratio 8

| Maximum Expulsion | Minimum Volume |

Figure2. Isosurfaces of eigenvalue contours for jet aspect ratio 8

is obtained by plotting the eigenvalue contours of the deformation matrix $\left(\dfrac{\partial u_i}{\partial x_j}\right)$. Notice that the spanwise width of the vortex rings along the long-axis of the jet decreases as the ring propagates downstream. This is not unexpected as the initial rectangular vortex ring is unstable and will undergo self-adjustment to acquire a more stable circular shape. Nevertheless it would be interesting to find out how the width of the vortex ring along the short-axis of the jet varies accordingly. Another interesting feature observed from these figures is that a freshly shed vortex ring tries to catch up with the train of vortices that has convected downstream, a phenomenon referred to as 'vortex-pairing'.

Figure 3 shows a sequence of snap-shots of vorticity contours in the *XZ*-plane (as viewed from the top). At short distance (4.2d) from the jet exit plane the vortex ring is almost rectangular and aligns with the rectangular jet exit plane (demarcated by the white dotted line), whose shape rapidly begins to change as the jet convects downstream. Within a distance of 12.4d from the exit plane the jet appears circular. But, this shape is short-lived as the jet is unstable and starts contracting in its own plane containing the long-axis and expanding in the plane containing short axis. This first occurs about 22.4d from the exit plane (showing up as a faint elliptical ring) which soon grows stronger and completely absorbs the circular ring aligning completely perpendicular to the rectangular exit plane. Being unstable again it begins to contract along the shorter axis and elongate along the longer axis. The process continues and the series of contours from a distance 39.9d to 57.4d depicts the continuous shape change that occurs. This kind of vigorous three-dimensional motion caused by vorticity self-rearrangement is known to be useful for enhanced mixing. The phenomenon is termed as 'axis-switching' and has been observed in steady jets from rectangular orifices. A corresponding crossflow case was analyzed with the same jet Reynolds number and a boundary layer Reynolds number, Re_δ = 424, with $\bar{V}_j/U_\infty$ = 0.5, δ/d = 2. Isosurfaces of eigenvalue contours for minimum ingestion phase during the expulsion portion of the cycle are shown in figure 4. Two views are presented which shows the hairpin-like vortex structures formed by the interaction of the external crossflow boundary layer with the vortex rings emerging for the jet exit.

y = 4.5d

y = 7.4d

y = 12.4d

y = 22.4d

y = 32.4d

y = 37.4d

y = 39.9d

y = 42.4d
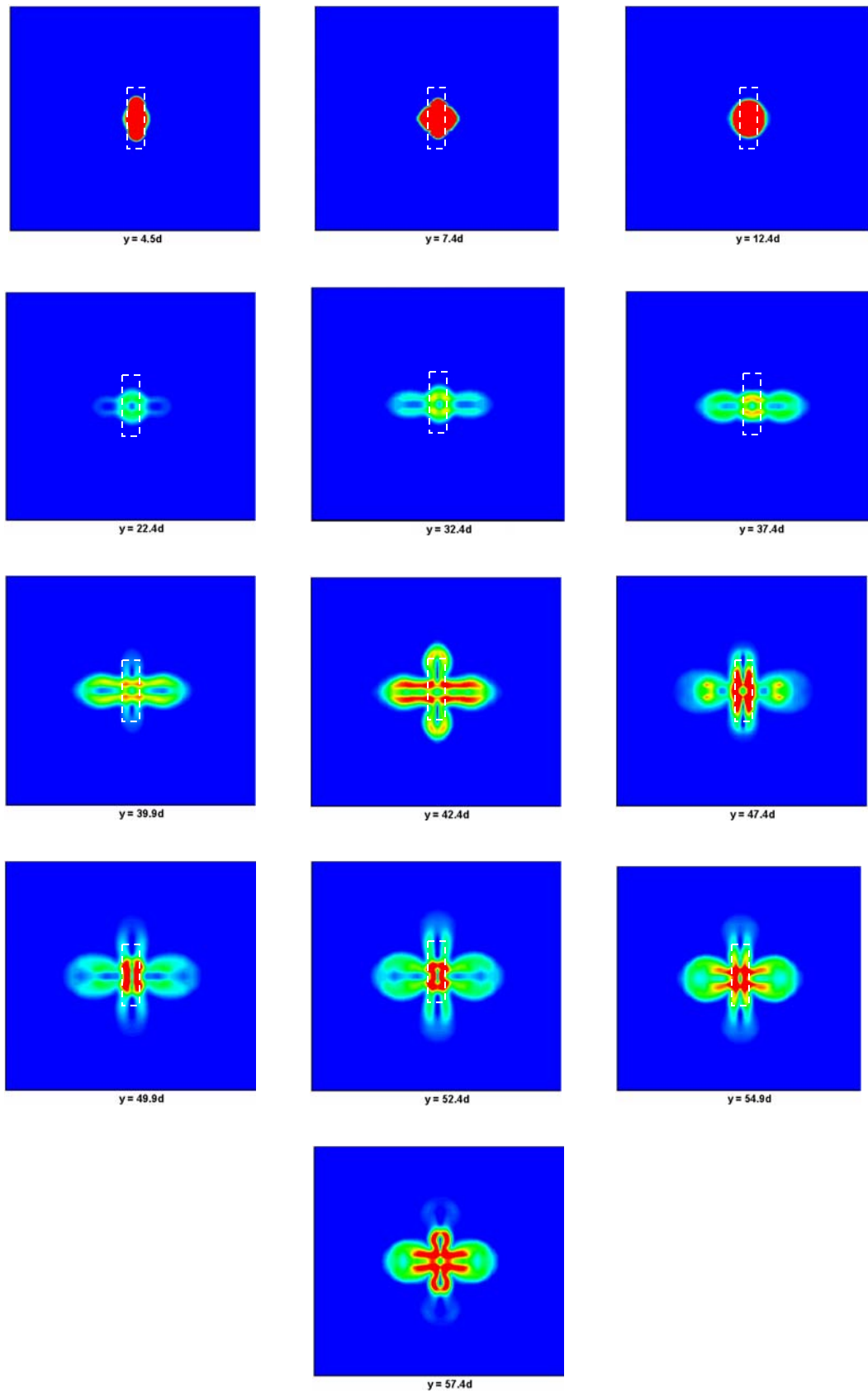
y = 47.4d

y = 49.9d

y = 52.4d

y = 54.9d

y = 57.4d

Figure 3 Time sequence of evolution of vorticity contours for synthetic jet with aspect ratio 8
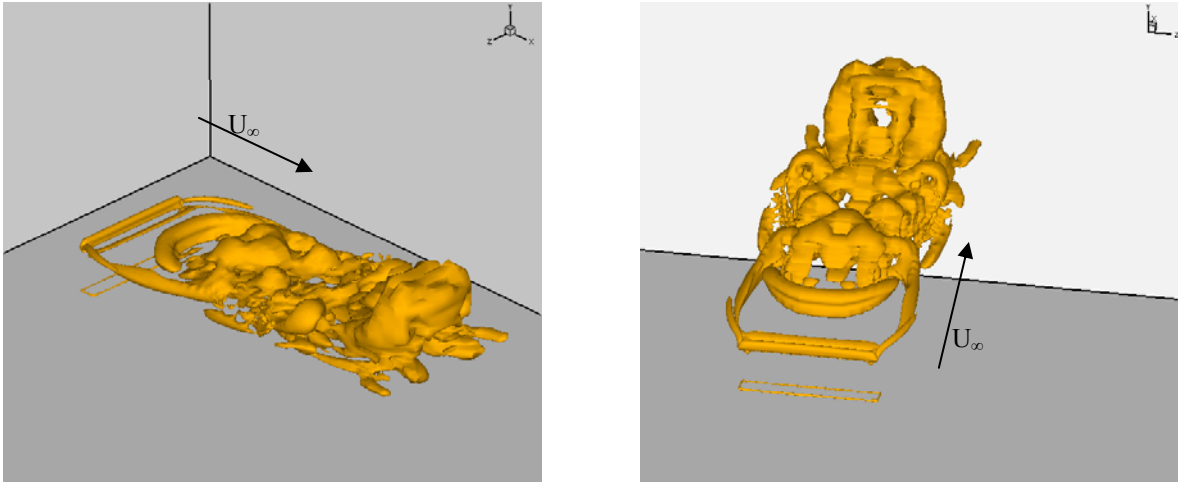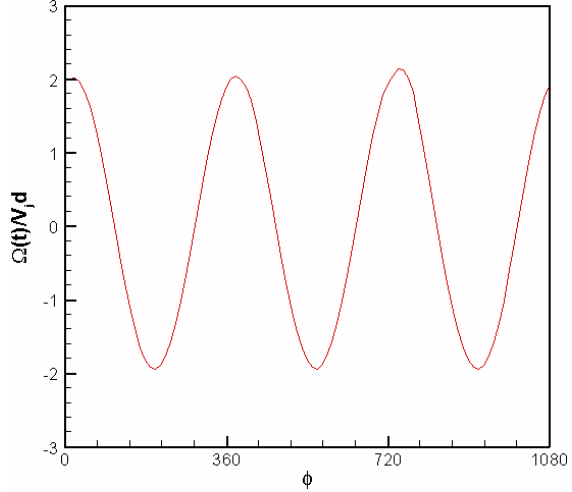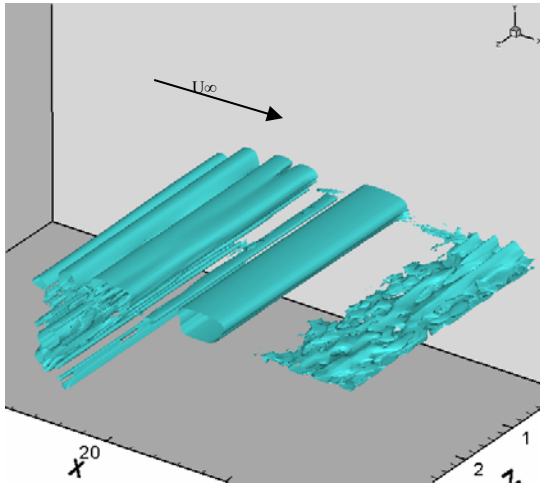
Figure 4 Isosurfaces of eigenvalue contours for a synthetic jet with aspect ratio 8 interacting with a external boundary layer.

Since, for aerodynamic applications, generally the external crossflow velocity is several times greater than the jet velocity, some computations have been made for $\bar{V}_j/U_\infty$ = 0.1. This would increase the boundary layer Reynolds number and therefore better and finer grids were needed. Also, these runs were made for the aspect ratio ∞ by applying the periodic boundary conditions at the spanwise boundaries. Initially some 2D cases were studied to fix a grid for this purpose and integral quantities of the jet such as the momentum coefficients and vorticity flux at the jet exit were examined to ensure grid independence of such quantities. The results are summarized in table 1 below.

Grid Size	Momentum Flux		Energy Flux		Vorticity Flux
	Expulsion	Ingestion	Expulsion	Ingestion	
195 x 128	2.012	1.7714	4.824	-3.6604	182.43
201 x 138	1.919	1.7715	4.425	-3.6574	176.94
% difference	4.8 %	0.005%	9.03 %	0.082%	3.1%
201 x 138	1.919	1.7715	4.425	-3.6574	176.94
207 x 148	1.944	1.759	4.523	-3.597	176.659
% difference	1.32 %	0.68 %	2.21 %	1.66 %	0.16 %

Table 1 Comparison of various integral jet quantities for refined grids

Note that 25% of grid points were increased only in the slot region in each of the above cases. Since the quantities agreed well for the second set of grids, a 201 x 138 x 33 grid was chosen for with Re_d=200, $\bar{V}_j/U_\infty$ = 0.1, δ/d = 2, giving Re_δ = 4000 for the corresponding 2D-3D case. It should be noted that unlike earlier runs, $\bar{V}_j$ =1 is fixed here. Figure 5 shows the isosurfaces of eigenvalue contour for the minimum volume phase. Note the large circular vortex in the downstream region formed with the interaction of the external flow.

| Isosurface of eigenvalue contour | Variation of vorticity flux with phase for 3 cycles |

Figure 5 Synthetic jet interacting with a external boundary layer (S=12, Re$_d$=200)

It was shown in earlier studies that vorticity flux, $\Omega_V = \int\limits_0^{T/2}\int\limits_0^{w/2}\int\limits_0^{d/2} \omega v\, dx\, dz\, dt$, $\omega = \sqrt{\omega_x^2 + \omega_y^2 + \omega_z^2}$, is an important parameter that determines the "formation" of synthetic jets in quiescent flow. Simple scaling arguments lead to the conclusion that the non-dimensional vorticity flux, is inversely proportional to the Strouhal number i.e., $\dfrac{\Omega_V}{\overline{V}_j d} = St^{-1} > K$, where K is a constant determined to be 2.0 and 0.16 for two-dimensional jets and axisymmetric jets, respectively. It is possible, however, parameters such as vorticity flux, might also play an important role in determining the effect of the jet on external flow. Experiments have shown a linear dependence for the vorticity flux with the Strouhal number. A similar relationship is shown to exist for two-dimensional jets interacting with a crossflow (Reni Raju et.al). Computations are being performed for three-dimensional jets interacting with external boundary layer for a range of Strouhal numbers fixing the parameters as mentioned above. The Strouhal number is varied by varying the Stokes number. Currently, computations are completed for S = 12, 24. A plot of the vorticity flux as a function of phase for three cycles is shown in figure for S = 12 case. The flux is normalized with average jet exit velocity and the jet width. The vorticity magnitude computed from the above integral for the both these cases are presented in the table 2 below. It is clear that as the Strouhal number increases the non-dimensional vorticity flux decreases thereby tending to give a linear relationship.

Strouhal Number	0.72	2.88
Vorticity Magnitude ($\Omega_V / \overline{V}_j d$)	5.66	1.39

Table 2

1.3 Time-Accurate Three-Dimensional Simulations of Synthetic Jets in Quiescent Air

The unsteady evolution of transitional synthetic jet in the absence of cross-flow is investigated by time-accurate three-dimensional direct numerical simulations of incompressible Navier-Stokes equations on Cartesian grids. Simulations are carried out at a Reynolds number ($\mathrm{Re} = \overline{V}_j d / \upsilon$) of 1150 and Stokes number ($St = \sqrt{2\pi f d^2 / \upsilon}$) of 17. The study models the flow inside the cavity using an oscillatory velocity boundary condition prescribed at the bottom of the cavity in order to generate a natural flow at the slot exit. The flow configuration is similar to the one studied by Yao et al. (2004) and the results from the computations are validated using their measurements to assess various aspects of the predictions. The effects of three-dimensionality, grid resolution and spanwise domain size on the predictions are studied systematically by a sequence of carefully designed computations detailed in Table 3. The results indicate that near the jet exit plane, the flowfield is dominated by the formation of counter-rotating vortex pairs that breakdown due to the onset of spanwise instabilities and transition to fully developed turbulent jet at short distances from the orifice.

Case	$L_x \times L_y \times L_z$	$N_x \times N_y \times N_z$
1	40d x 42.45d x 3.0d	132x 220 x 16
2	40d x 42.45d x 3.0d	132 x 220 x 24
3	40d x 42.45d x 4.5d	132 x 220x 24
4	60d x 60d x 6.0d	142 x 230 x 48

Table 3

Contours of phase-averaged spanwise vorticity obtained for Case 4 are plotted in figure 6. Phase angle φ = 0° is arbitrarily chosen to correspond to the commencement of the upward motion of the diaphragm modeled here by the pulsatile velocity boundary condition at the bottom of the cavity. At φ = 0°, the plot shows some remnants of the previous vortex pair in the near-field and the separation of the shear layer in the interior of the slot caused by the suction of the ambient fluid into the cavity before the upward motion of the diaphragm began. At 45° in phase, a new vortex pair is seen to roll up at the edges of the slot and its size is of the order of the slot width. The plot also shows separation of the shear layer at the inner edges of the slot. At φ = 90°, the roll-up of a new vortex pair is completed and the vortex pair detaches from the exit plane and grows in size as it advects downstream. At φ = 135°, small-scale structures begin to appear on the rim of vortex pairs. Also, the rollup of the shear layer at the inner lips of the slot advects downstream leading to Kelvin-Helmholtz-type instabilities that mark the first stage in the transition process. The expulsion phase is completed and the ingestion phase is commenced at φ = 180°, by which time the vortex pair has advected sufficiently downstream that it is not affected by the suction of ambient fluid into the cavity. At this juncture, the vortex pair loses coherence and begins to mix with the ambient fluid. At φ = 225°, the vortices lose their individual identity, and the suction generates vortex rollup in the interior of the cavity. At maximum-ingestion phase of 270°, the mixing of the primary vortex pair is complete, resulting in a fully developed turbulent jet beyond *y/d* = 3. The vortex pair inside the cavity as seen at φ = 315° starts to grow in size while it descends and engulfs the cavity before the next cycle is begun. Figure 7 on the following page shows the cross stream distributions of phase-averaged *u-* and *v-*velocities above the jet exit plane at y/d = 0.787, 1.575 and 2.362 at the maximum expulsion phase φ = 90°. Except for the lower values of the maxima and the minima in the *U*-velocity at y/d = 0.787 and the

V-velocity at y/d = 1.575 as compared to the measurements, the computed profiles closely agree with the experimental measurements. Figure 8 shows the cross stream distributions of the time-averaged *u-* and *v-*velocity profiles at three stations (y/d = 0.787, 1.575 and 2.362) above the jet exit plane. While the computed <u>-velocity profiles consistently show higher values than the measurements outside the core region of the jet at all stations, the computed <v>-velocity profiles closely match with the experiments except for the lower values along the jet centerline as compared to the measurements.

$\Phi = 0^o$ $\Phi = 45^o$ $\Phi = 90^o$

$\Phi = 135^o$ $\Phi = 180^o$ $\Phi = 225^o$
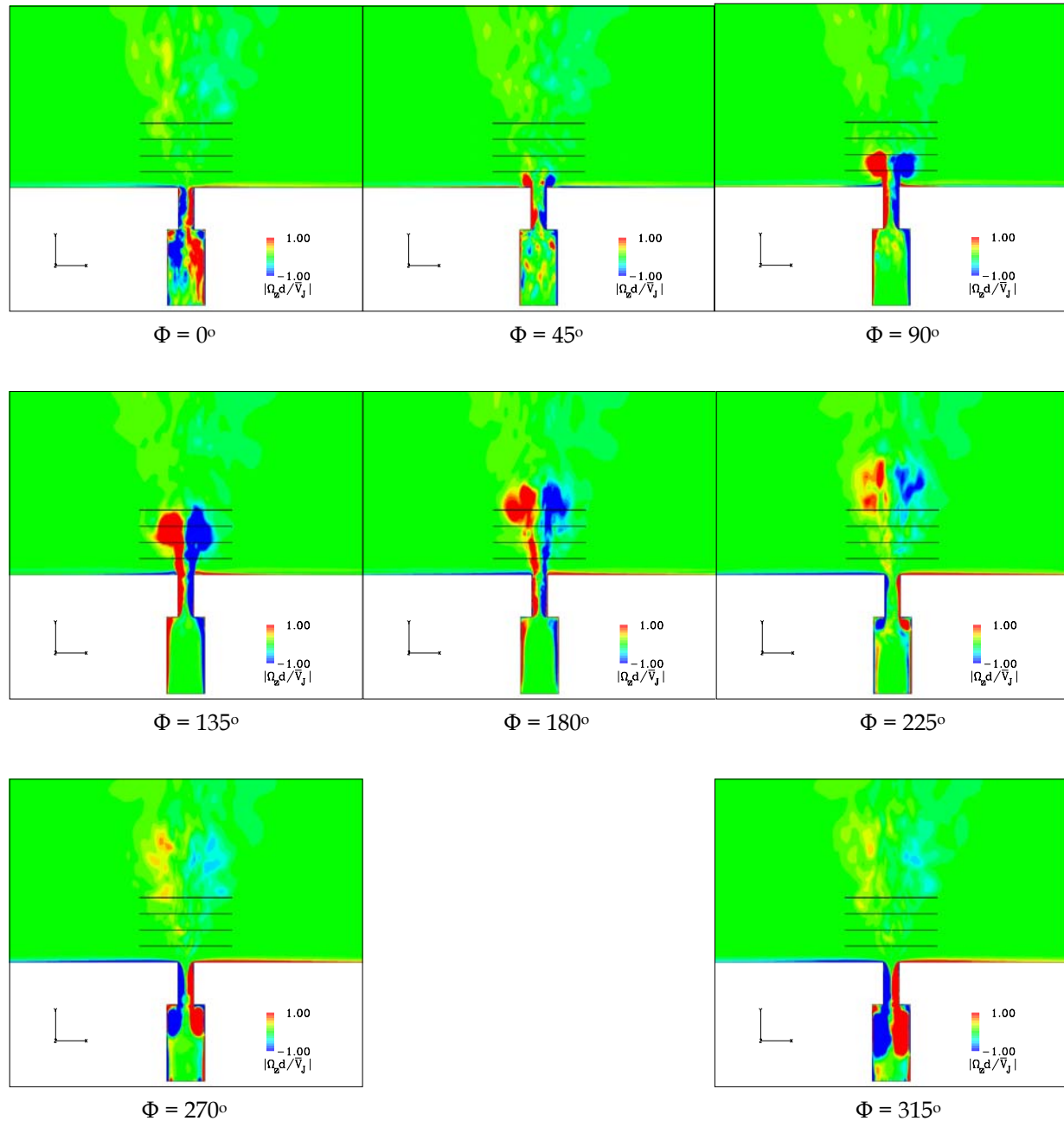
$\Phi = 270^o$ $\Phi = 315^o$

Figure 6 Contours of phase-averaged spanwise vorticity at various phase angles obtained for Case 4
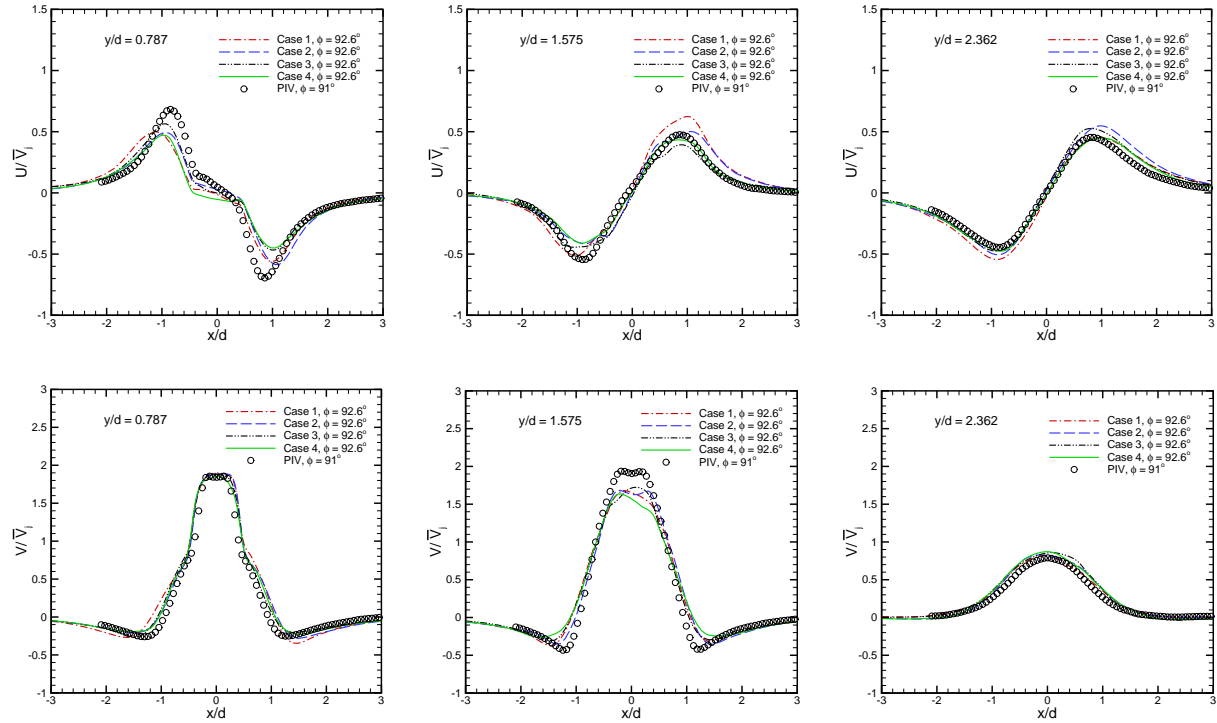
Figure 7 Plot of phase-averaged *u*- and *v*-velocity profiles along the horizontal lines *y/d* = 0.787, *y/d* = 1.574 and *y/d* = 2.362, above the jet exit plane at phase angle φ = 90º
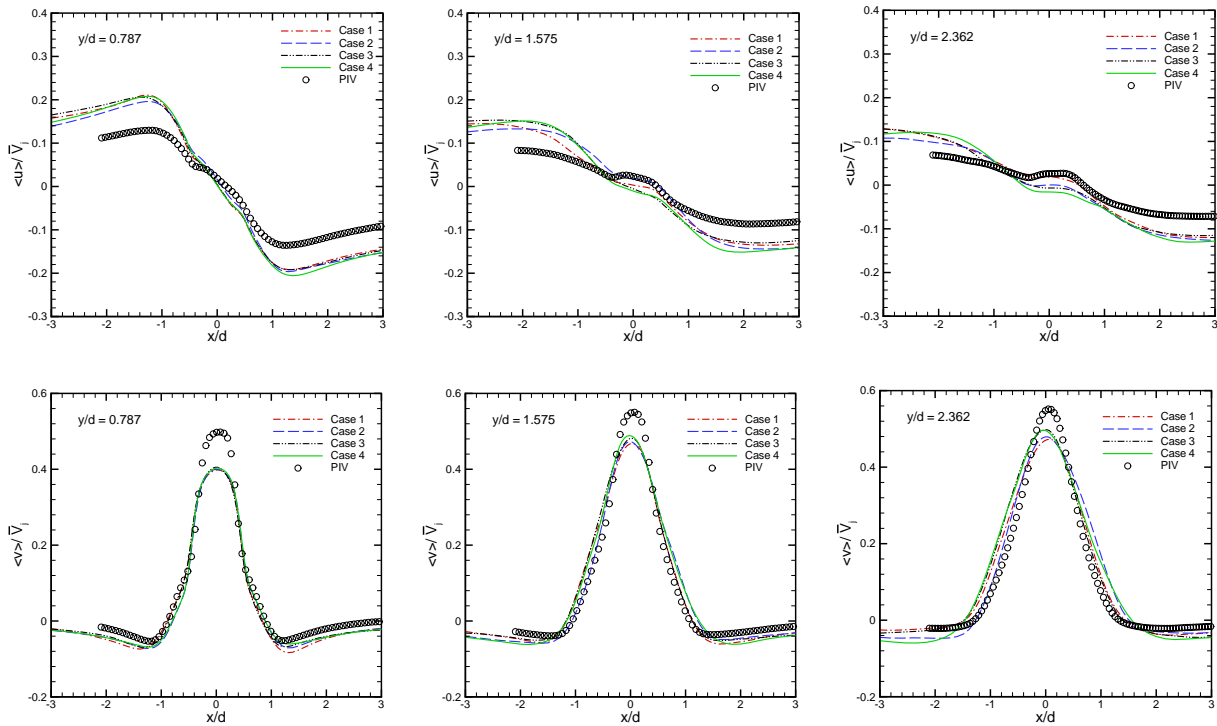

Figure 8 Plot of time-averaged *u*- and *v*-velocity profiles along the horizontal lines *y/d* = 0.787, *y/d* = 1.574 and *y/d* = 2.362, above the jet exit plane.

PUBLICATIONS RESULTING FROM THIS WORK

Kotapati, R. B., and Mittal, R. "Time-Accurate Three-Dimensional Simulations of Synthetic Jets in Quiescent Air," 43rd AIAA Aerospace Sciences Meeting and Exhibit, January 10-13, Reno, Nevada, AIAA Paper 2005-0103.

B R Ravi, Mittal, R., and Najjar, F. M., "Study of Three Dimensional Synthetic Flowfields using Direct Numerical Simulations.", AIAA Paper 2004-0091.

Mittal, R., Najjar, F. M., Byrganhalli, R., Seshadri, V., and Singh, H., "Simulation of Complex Biological Flows and Flow Control Problems on Cartesian Grids," Fifth International Conferences on Advances in Fluid Mechanics, March 2004, Lisbon, Portugal.

K A B Rupesh, B R Ravi, R Mittal, Q Gallas, and L Cattafesta, "Time-Accurate Numerical Simulations of Synthetic Jets in Quiescent Air," CFD Validation of Synthetic Jets and Turbulent Separation Control, NASA Langley Research Center Workshop, Williamsburg, VA, March 29-31, 2004.

Utturkar, Y., Holman, R., Mittal, R., Carroll, B., Sheplak, M., and Cattafesta, L., "A Jet Formation Criterion for Synthetic Jet Actuators," AIAA Paper 2003-0636.

Najjar, F. M., and Mittal, R., "Simulation of Complex Flows and Fluid-Structure Interaction of Fixed Cartesian Grids," FEDSM2003-45577, Proceedings of FEDSM'03, the 4th ASME-JSME Joint Fluids Engineering Conference, Honolulu, Hawaii July 6-11, 2003.

Udaykumar, H. S., Mittal, R., and Rampunggoon, P., "Interface Tracking Finite Volume Method for Complex Solid-fluid Interactions on Fixed Meshes," *Communications in Numerical Methods in Engineering*, 2002; 18: 89-97.

Mittal, R., and Rampunggoon, P., "On Virtual Aero shaping Effect of Synthetic Jets," Phys. of Fluids, Vol. 14, No.4, pp. 1533-1536, April 2002.

Utturkar, Y., Mittal, R., Rampunggoon, P., and Cattafesta, L., "Sensitivity of Synthetic Jets to the Design of Jet Cavity," AIAA Paper 2002-0124.

Mittal, R., Rampunggoon, P., and Udaykumar, H. S., "Interaction of a Synthetic Jet with a Flat Plate Boundary Layer," AIAA Paper 2001-2773.

THESES & DISSERTATIONS

Utturkar, Y, "Numerical Investigation of Synthetic Jet Flow Fields," M.S thesis, Department of Mechanical Engineering, University of Florida, 2002.

Rampunggoon, P., "Interaction of a Synthetic Jet with a Flat Plate Boundary Layer," Ph. D dissertation, Department of Mechanical Engineering, University of Florida, 2001.

References

1. Reni Raju, Rajat Mittal, Quentin Gallas, Louis Cattafesta (2005), Scaling of Vorticity Flux and Entrance

Length Effects in Zero-Net Mass-Flux devices, 35th AIAA Fluid Dynamics Conference and Exhibit, June 2005, Toronto, Onatario

2. Utturkar Y, Mittal R, Rampunggon P and Cattafesta L (2002), Sensitivity of Synthetic Jets to the Design of the Jet Cavity, AIAA 2002-0124, 40th AIAA Aerospace Sciences Meeting and Exhibit, Reno, NV

3. Yao, C. S., Chen, F. J., Neuhart, D., and Harris, J., "Synthetic Jets in Quiescent Air," *Proc. NASA LaRC Workshop on CFD Validation of Synthetic Jets and Turbulent Separation Control*, Williamsburg, Virginia, March 29-31, 2004.

4. Najjar, F. M., and Mittal, R., "Simulations of complex Flows and Fluid-Structure Interaction Problems on Fixed Cartesian Grids," FEDSM2003-45577, *Proc. FEDSM'03, 4th ASME-JSME Joint Fluids Engineering Conference*, Honolulu, Hawaii, 2003, pp. 184-196.

5. Ye, T., Mittal, R., Udaykumar, H.S., and Shyy, W., "An Accurate Cartesian Grid Method for Viscous Incompressible Flows with Complex Immersed Boundaries," *J. Comp. Phys.*, Vol. 156, 1999, pp. 18-33.

6. Zang, Y., Street, R. L., and Kossef, J. R., "A Non-staggered Grid, Fractional Step Method for Time-Dependent Incompressible Navier-Stokes Equations in Curvilinear Coordinates," J. Comp Phys., Vol. 114, 1994, pp. 18-33.

7. Leonard, B. P., "A Stable and Accurate Convection Modeling Procedure Based on Quadratic Upstream Interpolation," Comput. Methods Appl, Mech. Engrg., Vol. 19, 1979, pp. 59-98.